

Electronic structure investigation of GdNi using x-ray absorption, magnetic circular dichroism, and hard x-ray photoemission spectroscopy

C. W. Chuang¹,[✉] H. J. Lin,¹ F. M. F. de Groot,² F. H. Chang,¹ C. T. Chen,¹ Y. Y. Chin,³ Y. F. Liao,¹ K. D. Tsuei,¹ J. Arout Chelvane,⁴ R. Nirmala,⁵ and A. Chainani¹

¹National Synchrotron Radiation Research Center, Hsinchu Science Park, Hsinchu 30076, Taiwan

²Inorganic Chemistry and Catalysis, Utrecht University, Universiteitsweg 99, 3584 CG Utrecht, The Netherlands

³Department of Physics, National Chung Cheng University, Chiayi 62102, Taiwan

⁴Defence Metallurgical Research Laboratory, Hyderabad 500 058, India

⁵Department of Physics, Indian Institute of Technology Madras, Chennai 600 036, India



(Received 21 October 2019; revised manuscript received 11 January 2020; accepted 3 March 2020; published 19 March 2020)

GdNi is a ferrimagnetic material with a Curie temperature $T_C = 69$ K which exhibits a large magnetocaloric effect, making it useful for magnetic refrigerator applications. We investigate the electronic structure of GdNi by carrying out x-ray absorption spectroscopy (XAS) and x-ray magnetic circular dichroism (XMCD) at $T = 25$ K in the ferrimagnetic phase. We analyze the Gd $M_{4,5}$ -edge ($3d-4f$) and Ni $L_{2,3}$ -edge ($2p-3d$) spectra using atomic multiplet and cluster model calculations, respectively. The atomic multiplet calculation for Gd $M_{4,5}$ -edge XAS indicates that Gd is trivalent in GdNi, consistent with localized $4f$ states. On the other hand, a model cluster calculation for Ni $L_{2,3}$ -edge XAS shows that Ni is effectively divalent in GdNi and strongly hybridized with nearest-neighbor Gd states, resulting in a d -electron count of 8.57. The Gd $M_{4,5}$ -edge XMCD spectrum is consistent with a ground-state configuration of $S = 7/2$ and $L = 0$. The Ni $L_{2,3}$ -edge XMCD results indicate that the antiferromagnetically aligned Ni moments exhibit a small but finite total magnetic moment ($m_{tot} \sim 0.12\mu_B$) with the ratio $m_o/m_s \sim 0.11$. Valence band hard x-ray photoemission spectroscopy shows Ni $3d$ features at the Fermi level, confirming a partially filled $3d$ band, while the Gd $4f$ states are at high binding energies away from the Fermi level. The results indicate that the Ni $3d$ band is not fully occupied and contradicts the charge-transfer model for rare-earth based alloys. The obtained electronic parameters indicate that GdNi is a strongly correlated charge-transfer metal with the Ni on-site Coulomb energy being much larger than the effective charge-transfer energy between the Ni $3d$ and Gd $4f$ states.

DOI: [10.1103/PhysRevB.101.115137](https://doi.org/10.1103/PhysRevB.101.115137)

I. INTRODUCTION

Intermetallic alloys consisting of rare-earth and transition-metal elements have played a very important role in the development of basic and applied solid-state physics and materials science [1–3]. More recently, many intermetallic alloys have shown promising magnetic refrigeration applications related to properties of magnetoresistance, the magnetocaloric effect, and magnetostriction [4–6]. The rare-earth $4f$ electrons in intermetallic alloys are usually considered to be localized, while the transition-metal d electrons are considered to be delocalized or itinerant. It is well established that in intermetallics, most rare-earth atoms normally exhibit trivalent ground states, except for Ce, Eu, Sm, and Yb, which can show mixed valency [1–3]. An important question that arises in such intermetallic alloys consisting of rare-earth and transition-metal elements is the behavior of element-specific magnetism.

While the rare-earth element is expected to show a local magnetic moment, the behavior of the transition-metal magnetic moment is not as clear. It is well known for many such alloys that when the concentration of the rare-earth ion increases, the magnetic moments of transition-metal ions get reduced [1]. In this picture, it is expected that the transition-metal $3d$ band will gradually get filled on increasing rare-earth ion content. This picture is called the charge-transfer model,

and it could successfully explain the properties of many, but not all, R_xM_y alloys (where $R =$ rare-earth and $M =$ Fe, Co, Ni, Cu) [1–3]. There are some known exceptions to this model, such as the alloy system Gd_xFe_{1-x} , with $0.1 \leq x \leq 0.4$ [7]. Also, for GdNi₂ with a ferrimagnetic $T_C = 85$ K, while it was initially concluded that Ni is nonmagnetic in samples prepared at ambient pressure, it was also shown that samples prepared under high pressures of 5–8 GPa showed a reduced $T_C \sim 60$ K which was attributed to holes in the Ni $3d$ band indicative of magnetic Ni ions [2,8,9]. These results suggest that the Ni $3d$ band is near a filling instability which can be controlled by sample preparation conditions such as high pressure, which results in creating holes in the Ni $3d$ band leading to Ni magnetic moments. Subsequently, an x-ray magnetic circular dichroism (XMCD) study showed a small but finite spin magnetic moment ($m_s = 0.14\mu_B$) for Ni ions in GdNi₂ [10]. In this work, we investigate the electronic structure of GdNi, which has also been debated with respect to the charge-transfer model as discussed in the following.

GdNi is a binary alloy which undergoes a magnetic transition around $T_C = 69$ K and exhibits a large magnetocaloric effect near T_C [11,12]. The magnetocaloric effect is the thermal response of a material when an external magnetic field is applied or removed under adiabatic conditions. The

crystal structure of GdNi is orthorhombic (CrB-type structure, space group $CmCm$, No. 63) and exhibits a trigonal prism arrangement with Gd atoms occupying the prism corners and Ni atoms positioned at the center of the prism [13–15]. Early studies on the magnetic moments of Ni in GdNi concluded that Ni was nonmagnetic since it was expected that the Ni 3*d* shell can be fully occupied by electrons donated by trivalent Gd ions [16,17]. However, later studies concluded Ni was magnetic, and the Gd moment was ferromagnetically aligned with Ni moments, effectively leading to an excess moment of $7.2\mu_B$ compared to the expected theoretical value of a saturation moment of $7\mu_B$ for an isolated Gd trivalent ion [18]. Based on band structure calculations, it was shown by Paudyal *et al.* [19] that Gd can have a 4*f* derived magnetic moment of $7\mu_B$ in GdNi, with Gd 5*d* electrons also showing a finite moment of $0.3\mu_B$ and Ni 3*d* electrons showing a moment of $-0.1\mu_B$. This implied that the Gd moment is antiferromagnetically aligned with Ni moments in GdNi. Paudyal *et al.* also showed that the anisotropic shifts in lattice constants are responsible for a large spontaneous linear magnetostriction effect of 8000 ppm along the *c* direction and GdNi can be classified as a giant magnetostriction compound.

From Ni $L_{2,3}$ -edge (2*p*-3*d*) XMCD experiments of GdNi carried out earlier [20], it was concluded that the spin magnetic moment of Ni is very small ($m_s \sim 0.1\mu_B$) and antiferromagnetically coupled to the magnetic moments of Gd. However, in making the estimate for spin moment from a sum rule analysis, the Ni 3*d* hole density was assumed to be that of GdNi₂, based on earlier work [10]. The main focus of this work is to quantify the Ni hole density and magnetic moment as well as electronic parameters for describing the electronic structure of GdNi. In this work, we address the hole density of the Ni 3*d* states as well as the magnetic moments associated with the Ni 3*d* and Gd 4*f* states in GdNi using x-ray absorption spectroscopy (XAS) and XMCD experiments combined with calculations and a sum rule analysis [21–25]. We confirm the trivalency of the Gd ions and consistency of the Gd XMCD with an $S = 7/2$ and $L = 0$ ground state. We also carry out bulk-sensitive hard x-ray photoemission spectroscopy (HAXPES) of the valence band of GdNi to clarify the character of the occupied density of states near the Fermi level. As is well known [26,27], HAXPES is a reliable bulk-sensitive probe of the intrinsic electronic structure of solids. The HAXPES valence band spectrum of GdNi shows Ni 3*d* features at the Fermi level indicating a partially filled 3*d* band, while the Gd 4*f* states are at high binding energies away from the Fermi level. The results indicate that GdNi contradicts the charge-transfer model for rare-earth-based alloys. The obtained electronic parameters indicate that GdNi is a strongly correlated charge-transfer metal in the Zaanen-Sawatzky-Allen scheme [28], with the Ni on-site Coulomb energy being much larger than the effective charge-transfer energy between the Ni 3*d* and Gd 4*f* states.

II. EXPERIMENTS

GdNi polycrystalline samples were made by an arc-melting method using high-purity constituent elements in an argon gas atmosphere. The samples were subsequently annealed at

1173 K for 12 h in an evacuated quartz tube. The samples were characterized by x-ray powder diffraction and were confirmed to be single phase. Magnetization measurements were carried out using a physical property measurement system (PPMS, Quantum Design), and the results confirmed a ferrimagnetic $T_C = 69$ K, as reported earlier [12]. In addition, the magnetization of GdNi tends to saturate above a critical field of about 1.5 T, and it does not show a spin-flop behavior [11,12].

XAS and XMCD measurements were carried out at the Dragon Beamline (BL 11A) of the Taiwan Light Source. The beamline is a bending magnet beamline, and the degree of circular polarization $p = 0.8$. The total electron yield (TEY) method was used to measure XAS and XMCD across the Gd $M_{4,5}$ edge (3*d*-4*f*) and Ni $L_{2,3}$ edge (2*p*-3*d*) with circularly polarized light and an applied field of ± 4 T. The circularly polarized x rays were incident normal to the sample surface, and the x-ray propagation axis was parallel (μ_+) or antiparallel (μ_-) to the applied magnetic field (± 4 T). We have used a clockwise circular polarization and a field of +4 and -4 T to obtain the XAS spectrum as a sum of μ_+ , μ_- , and μ_0 (μ_0 corresponds to an applied field perpendicular to the incident beam), and in the first approximation μ_0 is taken to be $\mu_0 = [(\mu_+) + (\mu_-)]/2$, as is standard procedure [21,23]. Thus, XAS is proportional to the average of the μ_+ and μ_- spectra.

The photon energy was calibrated using a reference NiO sample and Dy metal sample. The total energy resolution at the Ni 2*p*-3*d* edge was better than 0.2 eV for the XAS spectra, but for the XMCD spectra, due to the small XMCD signal expected for Ni in GdNi we used a larger slit size to enhance the spectral intensity at the cost of the energy resolution. The reduced energy resolution does not affect the sum rule analysis as the total spectral weight is conserved. For the XAS and XMCD measurements, the sample was polished *ex situ* and immediately inserted into the fast entry chamber and pumped down to an ultrahigh vacuum (UHV) of better than 8×10^{-10} mbar. The sample was cooled using a liquid-He flow-type cryostat, and the measurements were carried out at $T = 25$ K.

We monitored the stability of the Gd XMCD spectra, and the spectra were stable for about 8 h at $T = 25$ K. Beyond 8 h, the Gd XMCD signal got reduced a little. However, we could recover the XMCD signal after heating up the sample to $T = 300$ K and cooling again to $T = 25$ K. This indicated that the Gd XMCD signal was sensitive to adsorbed gases but did not change its magnetic and electronic structure and the surface could be refreshed by warming up to $T = 300$ K. In order to calibrate the energy and confirm the absence of oxidation, we simultaneously measured the Ni *L* edge of the NiO reference sample at $T = 300$ K in a chamber placed just before the main sample chamber. Similarly, we also measured the O *K*-edge XAS of the NiO reference sample and the O *K*-edge energy range on the GdNi sample. Since the main peak of NiO Ni *L* edge is at 851.8 eV, which is about 1.2 eV below the main peak of Ni *L* edge of GdNi at 853.0 eV and since we did not see any feature at 851.8 eV in the GdNi sample, we confirmed the absence of oxidation on the GdNi surface. Further, we could quantify the intensity of the O *K*-edge XAS intensity on the sample surface to be less than 3% compared to the NiO O *K*-edge signal. The measured spectra were corrected for the

degree of circular polarization and for saturation effects in the TEY mode [29].

Valence band HAXPES ($h\nu = 6500$ eV) measurements were carried out at $T = 80$ K at the Taiwan beamline BL12XU of SPring-8 in Hyogo, Japan. The sample was cooled using a liquid-N₂ flow-type cryostat. The overall energy resolution for HAXPES was 0.26 eV, as estimated from a fit to the Fermi edge of gold at $T = 80$ K, which was also used to calibrate the binding energy scale. For the HAXPES measurements, the sample was cleaved inside the UHV preparation chamber at a pressure of 5×10^{-9} mbar and transferred to the main chamber at 8×10^{-10} mbar for measurements. Although the probing depths of the HAXPES and TEY XAS are ~ 100 Å and ~ 25 Å [27,29], respectively, since the surfaces were free of oxidation and the XMCD signal compared well with earlier studies on scraped samples [20], the data quality is good and represents the intrinsic electronic structure of GdNi, as is borne out by the results presented in the following.

III. RESULTS AND DISCUSSION

Figure 1 shows the experimental and calculated Gd $M_{4,5}$ -edge ($3d-4f$) XAS spectra of GdNi, measured at $T = 25$ K in the ferrimagnetic phase of GdNi. The experimental XAS spectrum consists of the spin-orbit split M_5 and M_4 levels separated by about 29 eV. The M_5 main peak is observed at an incident photon energy of 1182.3 eV with additional weak features at 1186.8 and 1189.6 eV. The M_4 features consist of two peaks of nearly equal intensity which are positioned at a photon energy of 1211.4 and 1213.0 eV, and a very weak feature is seen at 1217 eV. We used atomic multiplet calculations using the CTM4XAS program [30] to confirm that Gd is trivalent in GdNi. In order to compare the experimental data with the calculations, we have subtracted out step functions from the M_5 and M_4 edges convoluted with a Gaussian to mimic the transitions from the $3d$ core state to continuum states. The height of the step functions was set to a ratio of

$M_5 : M_4$ equal to 6 : 4, according to the J value of the core hole state. Since the excitonic effect on the $4f$ states is at least 5 eV with respect to delocalized states, the step function was applied from 10 eV above the main peaks.

In Fig. 1, we have plotted two types of calculated spectra: One with a symmetric Lorentzian broadening and the other with an asymmetric Fano broadening. While all the spectral features are reproduced in both calculations, there are small differences between them and also small discrepancies compared to the experimental data. For the Lorentzian and Fano broadened spectra, the weak satellites of the M_5 edge are at photon energy positions slightly lower than the energies compared to the experiment. In contrast, for the M_4 edge, the satellite energy positions are in fair agreement, but the relative intensities of the multiplet tail at energies above 1215 photon energy are significantly lower in the Lorentzian broadened spectrum compared to the experiment. This is a general problem known from early work on $M_{4,5}$ -edge XAS spectra of rare earths, and it was shown that a Fano broadening leads to a better match with the M_4 edge experimental spectra [31–33]. As shown in the Fano broadened spectrum in Fig. 1, it is clear that the multiplet tail intensities above 1215 eV indeed show an improvement compared to the Lorentzian broadened spectrum. While the results confirm the trivalent state of Gd, the finite intensity at high photon energies due to Fano broadening points to a breakdown of the sum rules used for calculating the spin and orbital moments of the Gd ion and is discussed later with the XMCD spectrum in Fig. 4.

In Fig. 2, we show the experimental and calculated Ni $L_{2,3}$ -edge ($2p-3d$) XAS spectrum of GdNi measured at 25 K. First of all, it is noted that the spectrum is quite unlike the XAS spectrum of Ni metal. The experimental spectrum consists of spin-orbit split L_3 and L_2 features separated by an energy of 17 eV. The L_3 main peak occurs at an incident photon energy of 853.0 eV, and the L_2 main peak is observed at an incident photon energy of 869.95 eV. The L_3 main peak has satellite features at about 856.05 and 860.25 eV, while the L_2 main peak has weak shoulders at 873.7 and 877.55 eV.

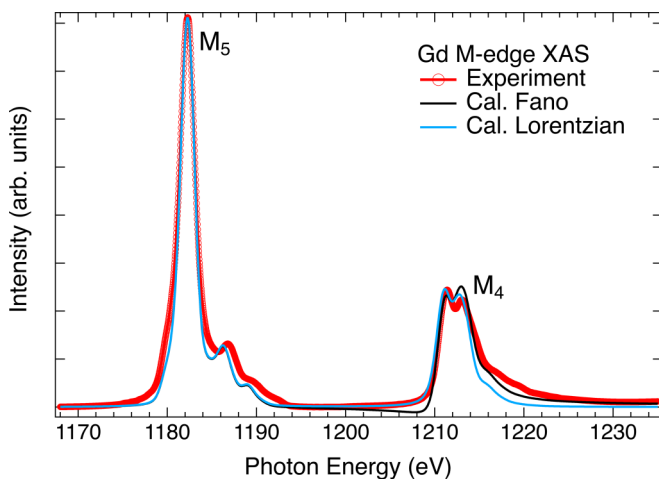


FIG. 1. The experimental Gd $M_{4,5}$ -edge ($3d-4f$) x-ray absorption spectrum of GdNi at $T = 25$ K compared with atomic multiplet calculations using two different types of broadenings: A Lorentzian broadening and a Fano broadening.

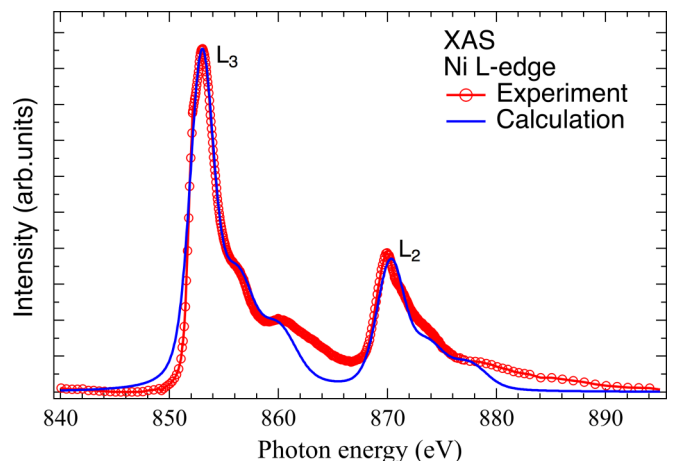


FIG. 2. The experimental Ni $L_{2,3}$ -edge ($2p-3d$) x-ray absorption spectra of GdNi at $T = 25$ K compared with a calculated spectrum obtained using a metal-ligand cluster model calculation.

We carried out calculations for the Ni $2p$ - $3d$ XAS using a NiL_6 ($L = \text{ligand}$) cluster model calculation using the QUANTY program [34–36]. We used a trigonal prism geometry with D_{3d} symmetry with a formal valency of divalent Ni ion. Although the real local structure of Ni is a regular trigonal prism corresponding to D_{3h} symmetry [13–15], we needed to use a lower D_{3d} symmetry to get the best match with the experimental data. This implies that the symmetry of the Ni trigonal prism has no mirror symmetry which is present in the D_{3h} point group. However, our model calculations reproduce all the features of the experimental data and can be considered a starting point to understand the Ni $L_{2,3}$ -edge ($2p$ - $3d$) XAS spectra.

The cluster model calculations were carried out by varying the electronic parameters in order to obtain a suitable match to the experimental spectrum. The best match was obtained for the Ni^{2+} configuration with the following electronic parameters: The charge transfer energy $\Delta = -0.6$ eV, the on-site Coulomb energy $U_{dd} = 6.2$ eV, the attractive core hole energy $U_{pd} = 10$ eV. The value of U_{dd} is typical for Ni-containing compounds, while U_{pd} is somewhat larger than what is normally used; for example, for NiO, $U_{dd} \sim 6.0$ eV, while $U_{pd} \sim 8.0$ eV [37]. The relatively large value of U_{dd} compared to Δ classifies GdNi as a strongly correlated charge-transfer metal in the Zaanen-Sawatzky-Allen (ZSA) scheme which is used to characterize Mott-Hubbard vis-a-vis charge-transfer systems in general [28]. The ZSA picture is used to characterize materials in terms of the relative values of the on-site Coulomb energy U_{dd} compared to the charge-transfer energy Δ scaled by the hybridization strength, which describes the nature of the lowest-energy excitations. When $U_{dd} < \Delta$, the material is called a Mott-Hubbard system with a d - d type lowest-energy excitation, while if $U_{dd} > \Delta$, it is called a charge-transfer system, where Δ is the charge-transfer energy determining the lowest-energy excitation. The charge-transfer energy Δ is usually defined as the energy separation between the $3d^n$ configuration and the charge-transferred $3d^{n+1}\underline{L}^1$ state, where \underline{L}^1 corresponds to one hole in ligand states. In our case, the ligand states are the Gd character nearest-neighbor states of the Ni site which transfer electrons to the Ni site. It is noted here that the charge-transfer model of intermetallic alloys is independent of the definition of the charge-transfer metal in the ZSA picture. The trigonal prism geometry of NiL_6 causes a crystal field splitting with three states: A high-energy doublet e_g' (d_{yz}, d_{zx}), an intermediate singlet a_{1g} ($d_{3z^2-r^2}$), and a low-energy doublet e_g'' ($d_{xy}, d_{x^2-y^2}$) [38,39]. The a_{1g} and e_g'' levels can be nearly degenerate or even inverted, depending on the valency as well as the spin-orbit interaction of the central metal ion Ni [39]. The energy separation between e_g' and a_{1g} was taken to be $D_{10} = 0.45$ eV, while the energy separation between a_{1g} and e_g'' was taken to be $D_{02} = 1.0$ eV, and the hybridization strengths of the d levels with the ligand states were set to $V_{a_{1g}} = -2.4$ eV, $V_{e_g'} = 0.65$ eV, $V_{e_g''} = -2.0$ eV. A Lorentzian broadening of 0.4 eV full width at half maximum (FWHM) and an energy-dependent Gaussian broadening, with 2.0 eV FWHM for the main L_3 and L_2 peaks and 2.5 to 3.0 eV for the satellites, were used to calculate the spectrum. The calculated spectrum matches fairly well with the main peak and satellite structure observed in experiment, as shown in Fig. 2.

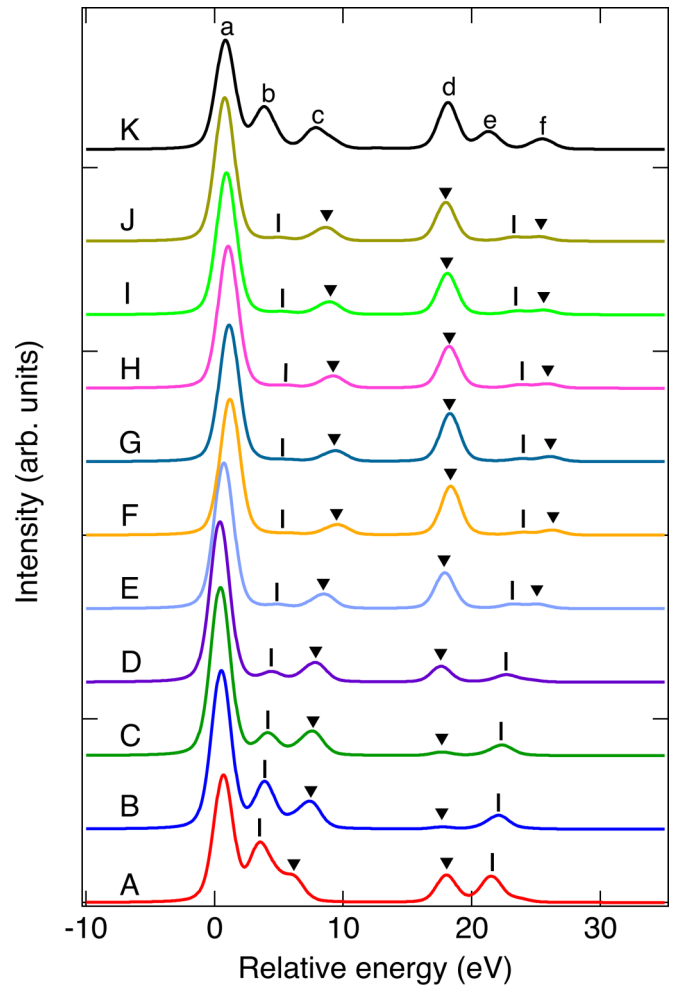


FIG. 3. A comparison of Ni $L_{2,3}$ -edge XAS spectra obtained using D_{3h} symmetry (spectra A–J) for different electronic parameters listed in Table 1 compared with the best match obtained using D_{3d} symmetry.

We would like to clarify that we first tried many calculations using the D_{3h} symmetry, as shown in Fig. 3 (spectra A to J). The best-match spectrum obtained with D_{3d} symmetry shown in Fig. 2 is also plotted in Fig. 3 as spectrum K, but with lower broadening parameters to clarify the differences (in Fig. 3, Gaussian broadening is set to 1.5 eV FWHM and Lorentzian broadening is 0.2 eV FWHM for all calculations). In contrast, spectrum A is the best-match spectrum we could obtain for D_{3h} symmetry, but it still fails to reproduce the experimental spectrum. In spite of an extensive search with many parameter sets with D_{3h} symmetry, we could not obtain a suitable calculated spectrum to match the experimental spectrum. In particular, if we got a suitable match for the L_3 edge, the L_2 edge did not match (see spectrum A in Fig. 3; electronic parameters: $U_{dd} = 7.2$ eV, $U_{pd} = 10.5$ eV, $\Delta = 0.2$ eV, $V_{a_{1g}} = -1.732$ eV, $V_{e_g'} = -0.5$ eV, $V_{e_g''} = -4$ eV). In contrast, if the main peaks of the L_3 and L_2 edges matched the experiment, the intensities of the satellite peaks were too low (see spectra E to J in Fig. 3).

In the following, we briefly describe our attempts to match the experimental spectrum using D_{3h} symmetry. Starting

TABLE I. Table of electronic parameters for calculated spectra shown in Fig. 3. Error bars for each electronic parameter which individually gives a d -electron count variation of about ± 0.02 , and acceptable changes in spectral shape are listed.

	Parameters					
	Δ	U_{dd}	U_{pd}	V_{alg}	$V_{eg'}$	$V_{eg''}$
Error bar	± 0.2	± 1	± 1	± 0.6	± 0.4	± 0.4
Spectrum						
A	0.2	7.2	10.5	-1.732	-0.5	-4.0
B	0.2	6.2	10.0	-1.732	-0.5	-4.0
C	-0.2	6.2	10.0	-1.732	-0.5	-4.0
D	-0.6	6.2	10.0	-1.732	-0.5	-4.0
E	-0.6	6.2	10.0	-2.0	-0.5	-4.0
F	-0.6	6.2	10.0	-2.4	-0.5	-4.0
G	-0.6	6.2	10.0	-2.4	0.0	-4.0
H	-0.6	6.2	10.0	-2.4	0.65	-4.0
I	-0.6	6.2	10.0	-2.4	0.0	-3.0
J	-0.6	6.2	10.0	-2.4	0.65	-2.0
K	-0.6	6.2	10.0	-2.4	0.65	-2.0

with the parameters of spectrum A, we changed U_{dd} and U_{pd} to the same value as used for spectrum K. We obtained spectrum B in which peaks b, c, d, and e got slightly shifted and the intensity of peak c increased, but the intensity of peak d got reduced. Spectra C and D were obtained by only changing Δ to -0.2 and 0.6 eV, respectively, keeping all other parameters as for spectrum B. The intensity of peaks b and f decreased, the intensity of peak d increased, and the positions of peaks b, c, and f got slightly shifted. Then, we changed the hybridization energy V_{alg} to -2 and -2.4 eV to obtain spectra E and F. We get a small new feature f, while the intensities of features b, e, and f are very weak. Also, the intensity of peak c decreased, and the intensity of peak d increased. All the peaks were slightly shifted to higher energy. In spectra G and H, only hybridization energy $V_{eg'}$ was changed to 0 and 0.65 eV, but the spectra hardly changed. Finally, the spectra I and J were obtained by changing hybridization energy $V_{eg'}$ to -3 and -2 eV, keeping all the other parameters fixed. The four spectra (G, H, I, J) are very similar. Thus, all the parameters of spectra J (D_{3h}) and K (D_{3d}) are the same, but clearly spectrum K matches better with the experimental spectrum. Hence, we felt using D_{3d} symmetry instead of D_{3h} symmetry, we could obtain a suitable match for energy positions and intensities of the L_3 and L_2 edges, as well as the satellites seen in the experimental spectrum. The calculated spectrum K corresponds to a Ni $3d$ electron count of 8.57 in the ground state. This indicates that the Ni $3d$ band is not fully occupied. In comparison, it is noted that from a magnetic study of a series of amorphous binary (GdFe, GdCo, and GdNi) and ternary alloys of the type $Gd_{0.2}(M1_xM2_{1-x})$, with $M1, M2 = Fe, Co, \text{ and } Ni$ and $x \sim 0.9$ to ~ 0.2 , it was concluded that GdNi corresponds to an effective one-electron transfer from Gd to Ni [40]. This would correspond to a total number of nine d electrons in GdNi, i.e., $3d^94s^2$ configuration, starting with $3d^84s^2$ for Ni metal. Our results indicate a lower estimate of 8.57 $3d$ electrons in the ground state in a configuration interaction picture, starting with a formal Ni^{2+} divalent

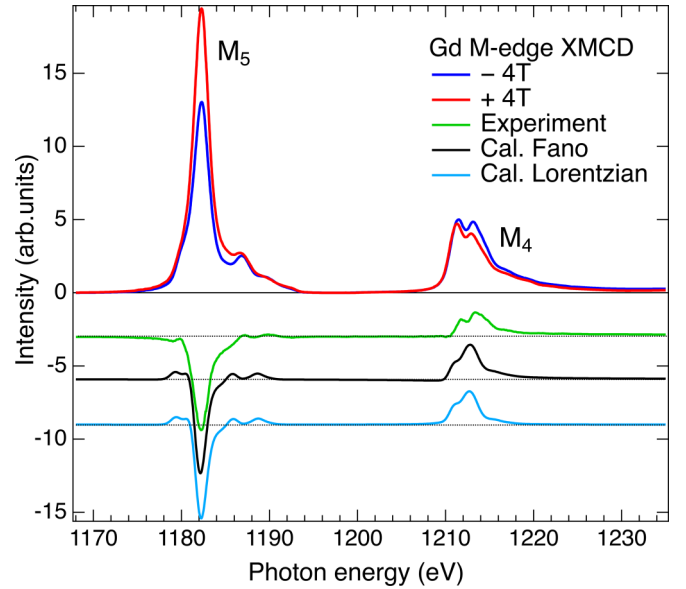


FIG. 4. The experimental Gd $M_{4,5}$ -edge ($3d-4f$) XMCD spectra of GdNi at $T = 25$ K compared with atomic multiplet calculations using two different types of broadenings: A Lorentzian broadening and a Fano broadening. The spectra are shifted along the y axis for clarity.

configuration of $3d^8$, and admixture from charge-transferred states of the type $3d^9\bar{L}^1$ and $3d^{10}\bar{L}^2$, where \bar{L} corresponds to a hole in the ligand states. As we show in the following, this results in a small magnetic moment for Ni sites, with slightly different values compared to the results reported by Yano *et al.* [20] However, in the study of Yano *et al.*, calculations for the XAS Ni $2p-3d$ and XMCD spectra were not reported. Thus, our results provide a direct and quantitative measure of the d electron count of Ni in GdNi.

In Fig. 4, we show the Gd $M_{4,5}$ -edge XMCD spectrum measured at $T = 25$ K, using circularly polarized x rays and an applied field of ± 4 T. The difference spectrum between the $+4$ and -4 T spectra shows a clear XMCD signal, as seen in Fig. 4. The spectral features are very similar to earlier XMCD spectra of GdNi [20], as well as other Gd-containing materials like GdNi₂ [10], Ce_{0.5}Gd_{0.5}Ni [41], the metallacrown materials GdNi₈ [42], etc. The similarity of the XMCD spectra in different materials indicates consistency with a localized picture for the Gd^{3+} ions. We have used the CTM4XAS program with the same electronic parameters as for the calculated XAS spectrum shown in Fig. 1 to also calculate the XMCD spectrum. Here again, we have calculated the XMCD spectra with a symmetric Lorentzian broadening and an asymmetric Fano broadening. The calculated XMCD spectra for both cases are very similar, indicating that although the XAS spectrum was better explained by the Fano broadened spectrum, the XMCD spectrum is not sensitive to the type of broadening used. The calculated XMCD spectra correspond to a ground-state configuration of $S = 7/2$ ($S_z = -3.465\mu_B$) and $L = 0$ ($L_z = -0.0345\mu_B$). L_z is not exactly zero due to a combination of $4f4f$ multiplet interactions and the $4f$ spin-orbit coupling. However, if we use a Fano broadening to simulate the XAS and XMCD spectra, this leads to a small dip before the M_4 edge and finite intensity at photon

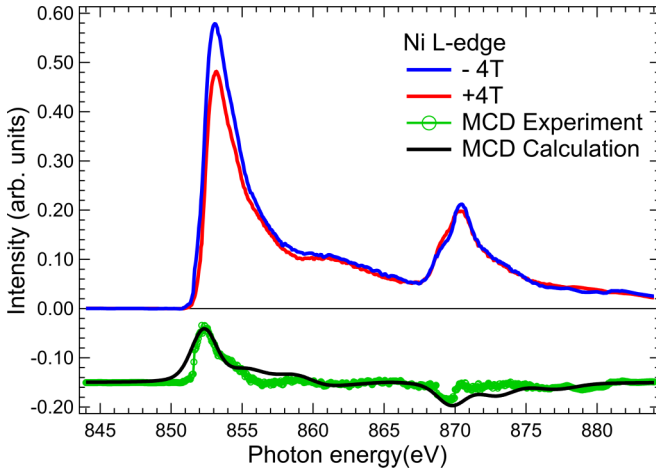


FIG. 5. The experimental Ni $L_{2,3}$ -edge ($2p$ - $3d$) x-ray magnetic circular dichroism spectra of GdNi at $T = 25$ K compared with the calculated spectrum obtained using a metal-ligand cluster model calculation. The spectra are shifted along the y axis for clarity

energies far above the M_4 edge in XAS and XMCD spectra. This means that we cannot set the XMCD intensity to zero before and after the edge. Further, the integral of the XAS and XMCD spectra does not saturate at high photon energies. In turn, this implies that the orbital magnetic moment m_o cannot be zero even for Gd^{3+} ions with $L = 0$, leading to an effective breakdown of the sum rule analysis [21–23]. It is interesting to test this proposition quantitatively on other rare-earth systems, and future work in this direction would be valuable. We have, nonetheless, carried out a sum rule analysis using the atomic multiplet calculation results and compared it with the experimental XAS and XMCD data. We first normalized the calculated XAS spectrum with the experimental spectrum. Using the same normalization factor for the theoretical XMCD intensity results in a higher intensity of the calculated spectrum compared to the experimental XMCD spectrum. The atomic calculation results need to be reduced to 92.6% in order to match the experimental XMCD spectrum. Based on this, the experimental estimate of the effective spin magnetic moment $m_{s,\text{eff}} = 2S_{z,\text{eff}} = 6.42 \pm 0.1\mu_B$; that is, it is reduced compared to the $7\mu_B$ corresponding to the $S = 7/2$ ground state. Similarly, the effective orbital magnetic moment was reduced to $m_{o,\text{eff}} = 0.032 \pm 0.01\mu_B$. We attribute the reduced effective spin moment $m_{s,\text{eff}}$ to the role of crystal field effects, the finite temperature of the measurement, and the fact that we needed a Fano-type broadening to better explain our experimental data for the multiplet tail intensities above 1215 eV (Fig. 1). It is noted that in a recent study on *in situ* deposited amorphous thin films of Co_xGd_{1-x} , a reduction of Gd spin moment with $m_s = 3.8\mu_B$ was reported [43].

Figure 5 shows the Ni XMCD spectra measured at $T = 25$ K, using circularly polarized X-rays and an applied field of ± 4 T. The data show a clear XMCD signal, as seen in the ± 4 -T difference spectrum. The sign of the Ni $L_{2,3}$ -edge ($2p$ - $3d$) XMCD results indicates that the Ni moments are antiferromagnetically aligned with the Gd moments. The Ni XMCD data are slightly different from those of Yano *et al.* for the main L_3 peak, which has a higher-energy weak shoulder

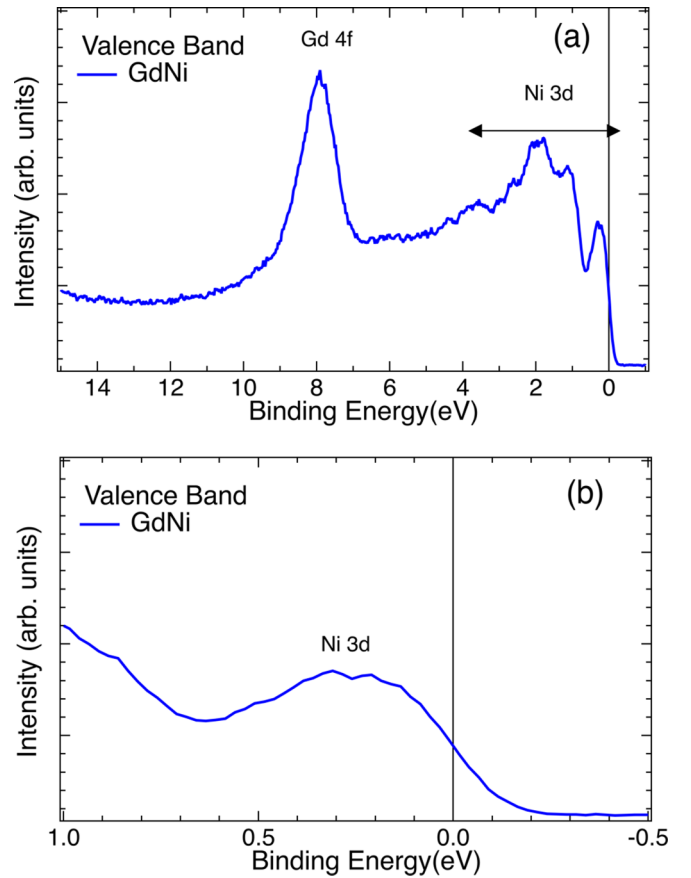


FIG. 6. (a) The experimental hard x-ray wide-valence-band photoemission spectrum of GdNi at $T = 80$ K shows the Gd $4f$ states at high binding energies and the Ni $3d$ -dominated states at the Fermi level and within 4-eV binding energy. (b) The near Fermi level region plotted on an expanded binding energy scale shows the Fermi level lies at the midpoint of the leading edge of the Ni $3d$ feature.

in our case but was a single peak in the work of Yano *et al.* [20]. However, our Ni XMCD data match well with the Ni XMCD data of fractured single-crystal $Ce_{0.5}Gd_{0.5}Ni$ reported by the same group later [41]. We have used the same electronic parameters as for the calculated XAS spectrum to also calculate the XMCD spectrum. As seen in Fig. 5, the calculated spectrum reproduces all the features of the XMCD experimental data, although the intensities of the weak features do not match well the calculations. We have estimated the spin and orbital magnetic moments m_s and m_o for Ni ions using a sum rule analysis [21–23], and we obtained $m_s = 0.11 \pm 0.01\mu_B$, $m_o = 0.012 \pm 0.01\mu_B$, giving $m_{\text{tot}} \sim 0.12 \pm 0.02\mu_B$. These values are slightly different than the previously estimated values of $m_s = 0.09\mu_B$ and $m_o = 0.014\mu_B$ [20]. It is also noted that Yano *et al.* reported the ratio $m_o/m_s = 0.16$ [20], and we obtain a ratio of $m_o/m_s = 0.11$.

Finally, in Figs. 6(a) and 6(b), we plot the wide valence band and the near Fermi level HAXPES spectrum of GdNi measured at $T = 80$ K, respectively. The HAXPES valence band of GdNi shows the Gd $4f$ states as a broad, intense peak centered at a high binding energy of 8 eV. Further, the Ni $3d$ -dominated states occur at the Fermi level and within 4-eV binding energy: A sharp peak is seen at 0.25-eV

binding energy [the near Fermi level spectrum is drawn on an expanded binding energy scale in Fig. 6(b)], followed by higher-intensity features at 1.1 and 2.0 eV and weak features at 2.7- and 3.5-eV binding energy. This assignment is qualitatively consistent with electronic structure calculations of the Ni 3d density of states obtained using a tight-binding linear muffin-tin orbitals method [44], although the sharp peak at the Fermi level observed in our experimental data occurs at about 1.3-eV binding energy in the calculations. The calculations further indicated that the Gd 4f occupied states occur at about 4.8-eV binding energy and the weaker intensity Gd 5d states are spread between the Fermi level and 5-eV binding energy. Hence, it is possible that the weak features at 2.7- and 3.5-eV binding energies may also have contributions from Gd 5d states which overlap the Ni 3d states. On the other hand, soft x-ray photoemission studies on several Gd-based intermetallics [45–49] containing Gd and Ni, such as GdNi_{5-x}Al_x, Gd₃Ni₈Al, GdNi₄B, GdNi₄Si, Gd(Ni_{1-x}Co_x)₃, and Gd(Ni_{1-x}Fe_x)₃, have shown a broad Gd 4f-derived feature at 8-eV binding energy, while the Ni 3d states occur between the Fermi level and about 4-eV binding energy. Our results indicate the strong similarity of the spectral features of Gd 4f and Ni 3d states as observed in the series Gd(Ni_{5-x}Al_x), Gd(Ni_{1-x}Co_x)₃, and Gd(Ni_{1-x}Fe_x)₃. However, one important difference in GdNi compared to Gd₃Ni₈Al, GdNi₄B, and GdNi₄Si is that we see a sharp lowest-binding-energy Ni 3d-derived feature at 0.25 eV cutting the Fermi level [Fig. 6(b)], while the lowest-binding-energy Ni 3d feature in Gd₃Ni₈Al, GdNi₄B, and GdNi₄Si is at about 1-eV binding energy and shows weak intensity at the Fermi level [46,47]. Our results thus indicate that the Ni 3d band occurs at the Fermi level and is partially occupied. While the Ni 3d states would participate in charge and thermal transport processes, the very small magnetic moment of Ni

in GdNi suggests it would result in a weak contribution to the magnetocaloric effect, while the large Gd spin moments would play a dominant role in the magnetocaloric properties of GdNi.

IV. CONCLUSION

In conclusion, we have carried out XAS and XMCD of GdNi in the ferrimagnetic phase at $T = 25$ K. The Gd $M_{4,5}$ -edge and Ni $L_{2,3}$ -edge XAS and XMCD spectra could be analyzed using atomic multiplet and cluster model calculations, respectively. The Ni $L_{2,3}$ -edge XAS and XMCD experimental spectra are fairly consistent with the cluster model calculations carried out for the D_{3d} local symmetry. We were able to quantify the hole density of the Ni 3d states as well as the magnetic moments associated with the Ni 3d states in GdNi. We also confirmed the trivalency of Gd ions and consistency of the Gd XMCD with an $S = 7/2$ and $L = 0$ ground state. The HAXPES valence band spectrum shows a Ni 3d character sharp peak at the Fermi level, consistent with a partially filled 3d band, while the Gd 4f states are at high binding energies away from the Fermi level. The results indicate that the Ni 3d band is not fully occupied and contradicts the charge-transfer model for rare-earth-based alloys.

ACKNOWLEDGMENTS

H.J.L. thanks the Ministry of Science and Technology of Taiwan, Republic of China, for financially supporting this research under Contract No. MOST 106-2112-M-213 -003 -MY3. A.C. thanks the Ministry of Science and Technology of Taiwan, Republic of China, for financially supporting this research under Contract No. MOST 108-2112-M-213-001-MY3.

- [1] K. N. R. Taylor, Intermetallic rare-earth compounds, *Adv. Phys.* **20**, 603 (1971).
- [2] W. E. Wallace, *Rare Earth Intermetallics* (Academic, New York, 1973).
- [3] K. H. J. Buschow, Rare earth compounds, in *Handbook of Ferromagnetic Materials*, edited by W. P. Wohlfarth (North-Holland, Amsterdam, 1980), Vol. 1, Chap. 4, pp. 297–414.
- [4] V. Provenzano, A. J. Shapiro, and R. D. Shull, Reduction of hysteresis losses in the magnetic refrigerant Gd₅Ge₂Si₂ by the addition of iron, *Nature (London)* **429**, 853 (2004).
- [5] O. Tegus, E. Bruck, K. H. J. Buschow, and F. R. de Boer, Transition-metal-based magnetic refrigerants for room-temperature applications, *Nature (London)* **415**, 150 (2002).
- [6] J. Liu, T. Gottschall, K. P. Skokov, J. D. Moore, and O. Gutfleisch, Giant magnetocaloric effect driven by structural transitions. *Nat. Mater.* **11**, 620 (2012).
- [7] R. C. Taylor, Magnetic properties of amorphous GdFe films prepared by evaporation, *J. Appl. Phys.* **47**, 1164 (1976).
- [8] A. Slebarski, Experimental analysis of the band structure of rare-earth-Laves phases, *J. Magn. Magn. Mater.* **66**, 107 (1987).
- [9] A. V. Tsvyashchenko, L. N. Fomicheva, E. N. Shirani, A. A. Sorokin, G. K. Rysasny, B. A. Komissarova, L. G. Shpinkova, Z. Z. Akselrod, O. I. Kochetov and V. N. Trofimov, Charge and magnetic states of Ni ions in the GdNi₂ Laves phase synthesized at different pressures, *Phys. Rev. B* **55**, 6377 (1997).
- [10] M. Mizumaki, K. Yano, I. Umehara, F. Ishikawa, K. Sato, A. Koizumi, N. Sakai and T. Muro, Verification of Ni magnetic moment in GdNi₂ Laves phase by magnetic circular dichroism measurement, *Phys. Rev. B* **67**, 132404 (2003).
- [11] P. Kumar, K. G. Suresh, A. K. Nigam, and O. Gutfleisch, Large reversible magnetocaloric effect in RNi compounds, *J. Phys. D* **41**, 245006 (2008).
- [12] R. Rajivgandhi, J. Arout Chelvane, S. Quezado, S. K. Malik and R. Nirmala, Effect of rapid quenching on the magnetism and magnetocaloric effect of equiatomic rare earth intermetallic compounds RNi (R = Gd, Tb and Ho), *J. Magn. Magn. Mater.* **433**, 169 (2017).
- [13] R. E. Walline and W. E. Wallace, Magnetic and Structural Characteristics of Lanthanide-Nickel Compounds, *J. Chem. Phys.* **41**, 1587 (1964).
- [14] S. C. Abrahams, J. L. Bernstein, R. C. Sherwood, J. H. Wernick, and H. J. Williams, The crystal structure and magnetic properties of the rare-earth nickel (RNi) compounds, *J. Phys. Chem. Solids* **25**, 1069 (1964).
- [15] D. Gignoux and J. C. Gomez-Sal, Magnetic properties and structures of the rare earth compounds RNi_{1-x}Cu_x with the FeB-type structure, *J. Magn. Magn. Mater.* **1**, 203 (1976).

- [16] I. Ursu and E. Burzo, Paramagnetic resonance of the gadolinium-nickel intermetallic compounds, *J. Magn. Reson.* **8**, 274 (1972).
- [17] C. A. Poldy and K. N. R. Taylor, A possible influence of 3d states on the stability of rare earth-rich rare earth-transition metal compounds, *Phys. Status Solidi A* **18**, 123 (1973).
- [18] R. Mallik, P. L. Paulose, E. V. Sampathkumaran, S. Patil, and V. Nagarajan, Coexistence of localized and (induced) itinerant magnetism and heat-capacity anomalies in $Gd_{1-x}Y_xNi$ alloys, *Phys. Rev. B* **55**, 8369 (1997).
- [19] D. Paudyal, Y. Mudryk, Y. B. Lee, V. K. Pecharsky, K. A. Gschneidner, Jr., and B. N. Harmon, Understanding the extraordinary magnetoelastic behavior in GdNi, *Phys. Rev. B* **78**, 184436 (2008).
- [20] K. Yano, I. Umehara, K. Sato, and A. Yaresko, Revelation of Ni magnetic moment in GdNi single crystal by soft X-ray magnetic circular dichroism, *Solid State Commun.* **136**, 67 (2005).
- [21] B. T. Thole, P. Carra, F. Sette, and G. van der Laan, X-Ray Circular Dichroism as a Probe of Orbital Magnetization, *Phys. Rev. Lett.* **68**, 1943 (1992).
- [22] P. Carra, B. T. Thole, M. Altarelli, and X. Wang, X-Ray Circular Dichroism and Local Magnetic Fields, *Phys. Rev. Lett.* **70**, 2499 (1993).
- [23] C. T. Chen, Y. U. Idzerda, H.-J. Lin, N. V. Smith, G. Meigs, E. Chaban, G. H. Ho, E. Pellegrin, and F. Sette, Experimental Confirmation of the X-Ray Magnetic Circular Dichroism Sum Rules for Iron and Cobalt, *Phys. Rev. Lett.* **75**, 152 (1995).
- [24] F. M. F. de Groot, X-ray absorption and dichroism of transition metals and their compounds, *J. Electron Spectrosc. Relat. Phenom.* **67**, 529 (1994).
- [25] A. Tanaka and T. Jo, Resonant 3d, 3p and 3s Photoemission in Transition Metal Oxides Predicted at 2p Threshold, *J. Phys. Soc. Jpn.* **63**, 2788 (1994).
- [26] C. S. Fadley, Hard X-ray photoemission with angular resolution and standing-wave excitation, *J. Electron Spectrosc. Relat. Phenom.* **190**, 165 (2013).
- [27] *Hard X-ray Photoelectron Spectroscopy (HAXPES)*, edited by J. C. Woicik, Springer Series in Surface Sciences Vol. 59 (Springer, Cham, 2016).
- [28] J. Zaanen, G. A. Sawatzky, and J. W. Allen, Band Gaps and Electronic Structure of Transition-Metal Compounds, *Phys. Rev. Lett.* **55**, 418 (1985).
- [29] R. Nakajima, J. Stohr, and Y. U. Idzerda, Electron-yield saturation effects in *L*-edge x-ray magnetic circular dichroism spectra of Fe, Co, and Ni, *Phys. Rev. B* **59**, 6421 (1999).
- [30] E. Stavitski and F. M. F. de Groot, The CTM4XAS program for EELS and XAS spectral shape analysis of transition metal *L* edges, *Micron* **41**, 687 (2010).
- [31] U. Fano, Effects of Configuration Interaction on Intensities and Phase Shifts, *Phys. Rev.* **124**, 1866 (1961).
- [32] B. T. Thole, G. van der Laan, J. C. Fuggle, G. A. Sawatzky, R. C. Karnatak, and J.-M. Esteve, 3d x-ray-absorption lines and the $3d^9 4f^{n+1}$ multiplets of the lanthanides, *Phys. Rev. B* **32**, 5107 (1985).
- [33] J. B. Goedkoop, B. T. Thole, G. van der Laan, G. A. Sawatzky, F. M. F. de Groot, and J. C. Fuggle, Calculations of magnetic x-ray dichroism in the 3d absorption spectra of rare-earth compounds, *Phys. Rev. B* **37**, 2086 (1988).
- [34] M. W. Haverkort, M. Zwierzycki, and O. K. Andersen, Multiplet ligand-field theory using Wannier orbitals, *Phys. Rev. B* **85**, 165113 (2012).
- [35] Y. Lu, M. Hoppner, O. Gunnarsson, and M. W. Haverkort, Efficient real-frequency solver for dynamical mean-field theory, *Phys. Rev. B* **90**, 085102 (2014).
- [36] M. Haverkort, G. Sangiovanni, P. Hansmann, A. Toschi, Y. Lu, and S. Macke, Bands, resonances, edge singularities and excitons in core level spectroscopy investigated within the dynamical mean-field theory, *Europhys. Lett.* **108**, 57004 (2014).
- [37] M. A. van Veenendaal and G. A. Sawatzky, Nonlocal Screening Effects in 2p X-Ray Photoemission Spectroscopy Core-Level Line Shapes of Transition Metal Compounds, *Phys. Rev. Lett.* **70**, 2459 (1993).
- [38] R. Huisman, R. de Jonge, C. Haas, F. Jellinek, Trigonal-prismatic coordination in solid compounds of transition metals, *J. Solid State Chem.* **3**, 56 (1971).
- [39] T. Burnus, Z. Hu, H. Wu, J. C. Cezar, S. Niitaka, H. Takagi, C. F. Chang, N. B. Brookes, H.-J. Lin, L. Y. Jang, A. Tanaka, K. S. Liang, C. T. Chen, and L. H. Tjeng, X-ray absorption and x-ray magnetic dichroism study on Ca_3CoRhO_6 and Ca_3FeRhO_6 , *Phys. Rev. B* **77**, 205111 (2008).
- [40] R. C. Taylor and A. Gangulee, Magnetic properties of the 3d transition metals in the amorphous ternary alloys: $Gd_{0.2}(Fe_xCo_{1-x})_{0.8}$, $Gd_{0.2}(Co_xNi_{1-x})_{0.8}$, and $Gd_{0.2}(Fe_xNi_{1-x})_{0.8}$, *Phys. Rev. B* **22**, 1320 (1980).
- [41] T. Okane, Y. Takeda, K. Yano, A. Fujimori, H. Yamagami, K. Nishimura, Y. Isikawa, and K. Sato, X-ray Magnetic Circular Dichroism Study of $Ce_{0.5}Gd_{0.5}Ni$, *JPS Conf. Proc.* **3**, 011028 (2014).
- [42] A. Alhassanat, L. Volker, C. Gamer, A. Rauguth, A. Kredel, C. Luo, F. Radu, A. A. Sapozhnik, T. Mashoff, E. Rentschler, and H. J. Elmers, Solvent-induced high-spin transition in double-decker 3d-4f metallocrowns, *Phys. Rev. B* **99**, 104404 (2019).
- [43] N. Bergeard, A. Mougín, M. Izquierdo, E. Fonda, and F. Sirotti, Correlation between structure, electronic properties, and magnetism in Co_xGd_{1-x} thin amorphous films, *Phys. Rev. B* **96**, 064418 (2017).
- [44] J. Ruzs, I. Turek, and M. Divis, Random-phase approximation for critical temperatures of collinear magnets with multiple sublattices: GdX compounds ($X = Mg, Rh, Ni, Pd$), *Phys. Rev. B* **71**, 174408 (2005).
- [45] M. Coldea, S. G. Chiuzbaian, M. Neumann, D. Todoran, M. Demeter, R. Tetea, and V. Pop, Magnetic and Electronic Properties of $GdNi_{5-x}Al_x$ Intermetallic Compounds, *Acta Phys. Pol. A* **98**, 629 (2000).
- [46] V. Pop, M. Coldea, M. Neumann, S. Chiuzbaian, and D. Todoran, X-ray photoelectron spectroscopy and magnetism of Gd_3Ni_8Al , *J. Alloys Compd.* **333**, 1 (2002).
- [47] A. Kowalczyk, A. Szajek, M. Falkowski, and G. Chelkowska, Magnetic properties and electronic structure of $GdNi_4Si$ compound, *J. Magn. Magn. Mater.* **305**, 348 (2006).
- [48] M. Kwiecien, G. Chelkowska, and K. Rabiasz, Electronic structure, magnetic and electric properties of $Gd(Ni_{1-x}Co_x)_3$ compounds, *J. Alloys Compd.* **423**, 55 (2006).
- [49] A. Bajorek, A. Chrobak, G. Chelkowska, and M. Kwiecien, Influence of Fe substitution on the structure and magnetic properties in $Gd(Ni_{1-x}Fe_x)_3$ intermetallic compounds, *J. Alloys Compd.* **485**, 6 (2009).